Journal of Semiconductors
JOS iopscience.iop.org/jos
www.jos.ac.cn

Improving electrical performance and fringe effect in p-type SnO_x thin film transistors via Ta incorporation

Yu Song, Runtong Guo, Ruohao Hong, Rui He, Xuming Zou, Benjamin Iiguez, Denis Flandre, Lei Liao, and Guoli Li

Citation: Y Song, R T Guo, R H Hong, R He, X M Zou, B Iiguez, D Flandre, L Liao, and G L Li, Improving electrical performance and fringe effect in p-type SnO_x thin film transistors via Ta incorporation[J]. *J. Semicond.*, 2025, 46(9), 092602.

View online: https://doi.org/10.1088/1674-4926/25010031

Articles you may be interested in

Performance enhancement of solution-processed InZnO thin-film transistors by Al doping and surface passivation

Journal of Semiconductors. 2022, 43(3), 034102 https://doi.org/10.1088/1674-4926/43/3/034102

Performance of hydrogenated diamond field-effect transistors on single and polycrystalline diamond

Journal of Semiconductors. 2020, 41(12), 122801 https://doi.org/10.1088/1674-4926/41/12/122801

Effect of charge trapping on electrical characteristics of silicon junctionless nanowire transistor

Journal of Semiconductors. 2022, 43(5), 054101 https://doi.org/10.1088/1674-4926/43/5/054101

Suitable contacting scheme for evaluating electrical properties of GaN-based p-type layers

Journal of Semiconductors. 2023, 44(5), 052802 https://doi.org/10.1088/1674-4926/44/5/052802

Radiation-hardened property of single-walled carbon nanotube film-based field-effect transistors under low-energy proton irradiation

Journal of Semiconductors. 2021, 42(11), 112002 https://doi.org/10.1088/1674-4926/42/11/112002

Homojunction structure amorphous oxide thin film transistors with ultra-high mobility

Journal of Semiconductors. 2023, 44(5), 052101 https://doi.org/10.1088/1674-4926/44/5/052101

关注微信公众号，获得更多资讯信息

Journal of Semiconductors, 2025, 46, 092602
DOI: 10.1088/1674-4926/25010031
CSTR: 32376.14.1674-4926.25010031

ARTICLES

Improving electrical performance and fringe effect in p-type SnO_x thin film transistors via Ta incorporation

Yu Song[1], Runtong Guo[1], Ruohao Hong[1], Rui He[1], Xuming Zou[1], Benjamin Iñiguez[3], Denis Flandre[4], Lei Liao[2], and Guoli Li[2, †]

[1]School of Physics and Electronics, Hunan University, Changsha 410082, China

[2]College of Semiconductor (College of Integrated Circuits), Hunan University, Changsha 410082, China

[3]Department of Electronics Engineering, Universitat Rovira I Virgili, Tarragona 43007, Spain

[4]Institute of Information and Communication Technologies, Electronics and Applied Mathematics, Université catholique de Louvain, Louvain-la-Neuve 1348, Belgium

Abstract: In this work, the incorporation of tantalum (Ta) into p-type metal-oxide (SnO_x) semiconductor film is investigated to improve the electrical characteristics and suppress the fringe effect of thin film transistors (TFTs). The Ta-doped SnO_x (SnO_x:Ta) film is deposited by radio-frequency (RF) magnetron sputtering with a Sn:Ta (3 at.%) target and thermally annealed at 270 °C for 30 min. Here, we observe that the SnO_x:Ta film presents increased crystallinity, reduced defect density (3.25×10^{12} $cm^{-2}\cdot eV^{-1}$), and widened bandgap (1.98 eV), in comparison with the undoped SnO_x film. As a result, the SnO_x:Ta TFTs exhibit a lower off-state current (I_{off}), an improved on/off current ratio (2.17×10^4), a remarkably decreased subthreshold swing (SS) by 41%, and enhanced device stability. Additionally, by introducing Ta dopants, the fringe effect as well as the impact of channel width-to-length ratio (W/L) on electrical performances of the p-type oxide TFTs can be effectively suppressed. These results shall contribute to further exploration and development of p-type SnO_x TFTs.

Key words: tin monoxide; p-type thin film transistors; Ta doping; fringe effect; on/off current ratio

Citation: Y Song, R T Guo, R H Hong, R He, X M Zou, B Iñiguez, D Flandre, L Liao, and G L Li, Improving electrical performance and fringe effect in p-type SnO_x thin film transistors via Ta incorporation[J]. *J. Semicond.*, 2025, 46(9), 092602. https://doi.org/10.1088/1674-4926/25010031

1. Introduction

Metal oxide (MO) semiconductors have garnered significant attention in various electronic device applications, including flexible displays[1], sensing[2], radio frequency identification[3], and memories[4]. Compared to the n-type MO, which have demonstrated their excellent mobility, high on/off current ratio, and good stability[5], performance of the p-type MO still lags behind. In the p-type Sn^{2+}-based MO, the 5*s* orbital of Sn^{2+} hybridizes with the O 2*p* orbital to form the valence band maximum (VBM), resulting in a small carrier effective mass and high hole mobility[6, 7]. Nonetheless, the unfavorable phase stability induced by transformation of Sn^{2+} and Sn^{4+} oxidation states and the narrow band gap are the main challenges, which hinders the high-quality deposition of SnO_x film and its further application, e.g. thin-film transistors (TFTs)[7]. In recent years, researchers have suggested introducing a third element such as nickel (Ni), tantalum (Ta), and kalium (K) to enhance the film quality, by widening the stability range, compensating native defects, and retaining the cation lone-pair states[8–11]. For example, Ni incorporation can significantly improve the field-effect mobility of the p-type SnO_x TFTs up to 11 $cm^2/(V\cdot s)$, showing an approximately tenfold enhancement compared to that of the typical p-type MO TFTs[9]. But, from another aspect, Ni doping also degrades off-state current of the SnO_x TFTs and leads to an on/off current ratio of 2×10^2, which is much lower than the current switch ratio (exceeding 10^7) in the n-type MO TFTs.

Currently, introducing Ta element into the binary compound SnO has been deeply considered to tune its electronic band gap, decrease the effective mass of holes and boost the phase stability[8, 11, 12]. Based on the first principles calculations, crystal structure of Sn–O–Ta can be changed via Ta incorporation, predicting a theoretical holes' mobility over 60 $cm^2/(V\cdot s)$[8]. The electrostatic interaction among Sn, O, and Ta atoms and the stable lattice structure result in the enhanced thermodynamic stability of the Sn^{2+} states. Moreover, the Sn^{2+}-based MO with Ta incorporation has a wider band gap, which overcomes the issue of small band gap in SnO and offers a reduced concentration of intrinsic carriers and a lower off-state current for TFTs. Although the Sn^{2+}-based MO with Ta incorporation has been proposed as a promising wide-band-gap p-type MO, based on these extensive computational simulations[8, 11, 13, 14], no report has shown the experimental synthesis and demonstrated its semiconducting characteristics.

In this work, we for the first time demonstrate Ta incorporation into the p-type SnO_x film, and investigate material property and device performance of the fabricated TFTs. Our results show that Ta doping can effectively reduce defect density, increase crystallinity, and enlarge band gap of the doped

Correspondence to: G L Li, liguoli_lily@hnu.edu.cn
Received 27 JANUARY 2025; Revised 21 MARCH 2025.
©2025 Chinese Institute of Electronics. All rights, including for text and data mining, AI training, and similar technologies, are reserved.

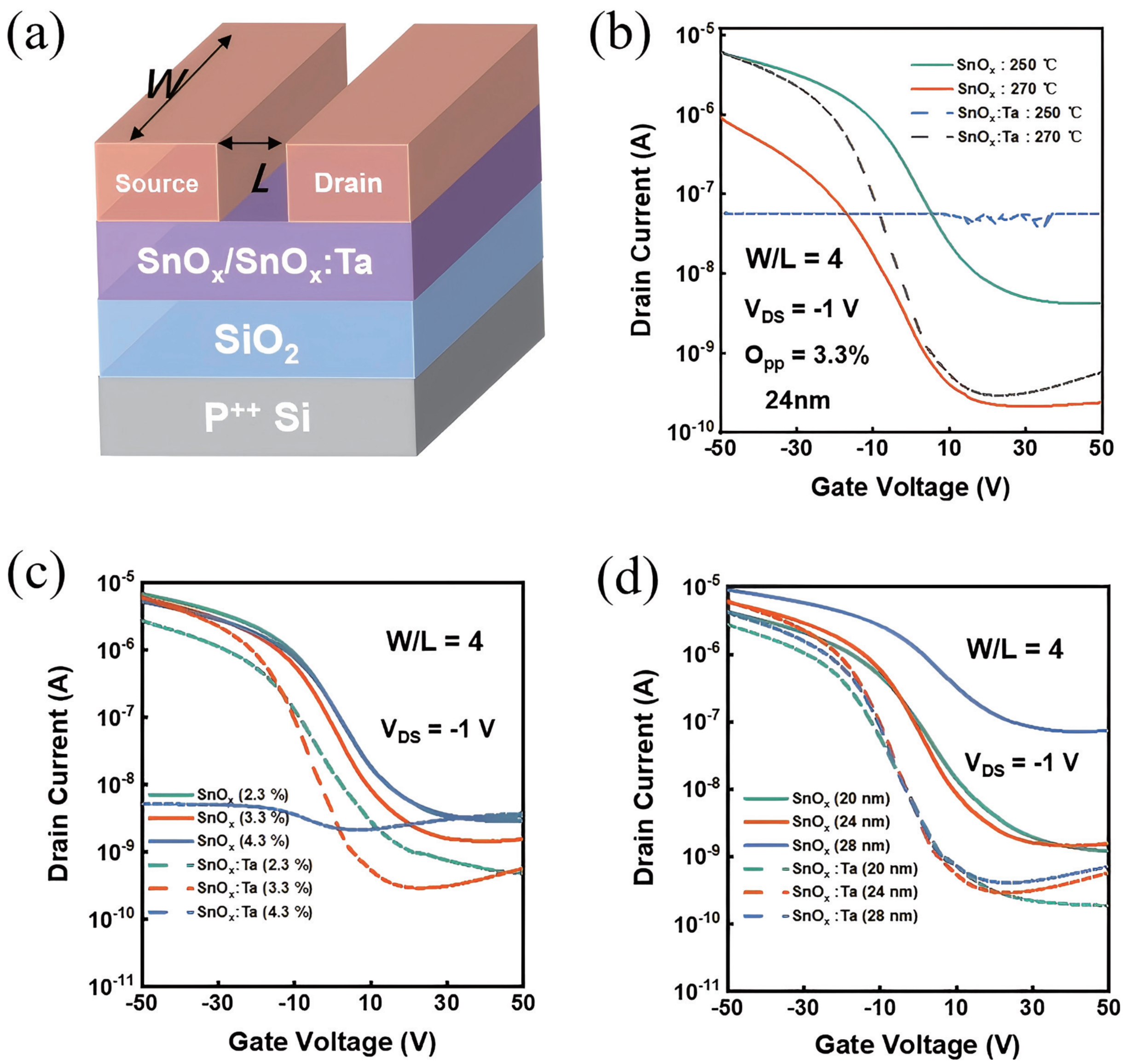

Fig. 1. (Color online) (a) Schematic structure of the SnO_x/SnO_x:Ta TFTs. Transfer curves (I_{DS}–V_{GS}) of the SnO_x and SnO_x:Ta TFTs, (b) after annealed at different temperature for 30 min, (c) deposited in an O_{PP} range of 2.3%–4.3%, (d) with a different channel thickness.

SnO_x film, optimizing electrical performance parameters such as field-effect mobility, on/off current ratio, subthreshold swing of the TFTs. Furthermore, the fringe effect is also improved for p-type SnO_x TFTs via Ta incorporation, as well as the device stability under prolonged negative bias stress (NBS) and negative bias temperature stress (NBTS).

2. Experiments

Fig. 1(a) illustrates schematic view of an inverted-staggered p-type MO TFTs, fabricated in this work. A heavily doped p-type silicon substrate was used as the bottom gate, with a 100 nm-thick SiO_2 layer thermally grown as the gate insulator. The SnO_x and SnO_x:Ta channel layers were deposited by RF magnetron sputtering from Sn and Sn:Ta (3 at.%) targets separately, in the atmosphere of O_2 and Ar mixture and at room temperature. During the sputtering, the RF power and the pressure inside the chamber are 30 W and 0.88 Pa, separately. Subsequently, the SnO_x and SnO_x:Ta films were separately annealed at 250 and 270 °C for 30 min in an ambient air to optimize the film quality. Next, the source and drain electrodes, with a 10 nm-thick Cr and 50 nm-thick Au layer, were formed through thermal evaporation. To investigate the fringe effect, several width-to-length (W/L) ratios have been designed for the SnO_x and SnO_x:Ta TFTs, with the fixed channel length of 30 μm and the deposited film area of 800 × 800 μm^2, by using the metal mask. Simultaneously, the metal–oxide–semiconductor capacitors (MOSCAPs) were fabricated to measure capacitance–voltage (C–V) and conductance–voltage (G–V) characteristics of the p-type MO active layers, by using an Agilent 4294A precision impedance analyzer at room temperature. Crystal structures, optical proper-

Table 1. Electrical parameters of the SnO_x/SnO_x:Ta TFTs deposited at O_{PP} = 3.3%.

Channel type	Channel thickness (nm)	μ_{FET} (cm²/(V·s))	SS (V/dec)	$I_{on/off}$
SnO_x	20	0.69	11.15	3.60×10^3
	24	0.97	9.21	4.13×10^3
	28	1.11	17.86	1.27×10^2
SnO_x:Ta	20	0.50	7.44	1.54×10^4
	24	1.12	7.19	2.13×10^4
	28	0.74	7.19	1.01×10^4

Table 2. Percentages of Sn^0, Sn^{2+}, Sn^{4+}, O_{Latt}, O_{Vac}, and O_{Chem} component by deconvoluting the XPS Sn 3*d* and O 1*s* profile.

Film	Sn^{+4}	Sn^{2+}	Sn^0	O_{Chem}	O_{Vac}	O_{Latt}
SnO_x (10 min)	58.47%	22.13%	19.40%	6.77%	78.14%	15.09%
SnO_x (30 min)	31.66%	49.18%	19.16%	76.41%	12.58%	11.01%
SnO_x:Ta (30 min)	25.12%	52.03%	22.85%	41.86%	20.07%	38.07%

ties, and chemical compositions of the SnO_x and SnO_x:Ta films were characterized by grazing incident X-ray diffraction (GIXRD), X-ray photoelectron spectroscopy (XPS) and ultraviolet–visible spectroscopy (UV–Vis) with a wavelength of 200–800 nm. Transfer characteristics and bias stability of the SnO_x and SnO_x:Ta TFTs were obtained using a semiconductor characterization system (Keithley 4200) in dark and atmospheric conditions. All the electrical parameters, including threshold voltage V_{th}, linear field-effect mobility μ_{FET}, and subthreshold slope SS, were extracted in the initial sweep while switching the TFTs from ON state to OFF state.

3. Results and discussion

As depicted in Fig. 1(b), the undoped SnO_x TFT achieves its optimal electrical performance after annealed at 250 °C for 30 min, whereas the doped SnO_x:Ta TFT presents its gate-control, semiconducting characteristic only after annealed at 270 °C. Here, the higher annealing temperature (20 °C) for SnO_x:Ta may be due to the difficulty of oxidizing Ta and the higher temperature requirement for Ta_2O_5 crystallization[2, 15, 16]. Oxygen partial pressure (O_{PP}) during the MO film deposition can also affect the fabricated TFT performance. In Fig. 1(c) O_{PP} ranges from 2.3% to 4.3%, both the SnO_x and SnO_x:Ta TFTs present the relatively superior characteristics at O_{PP} = 3.3% (red curves). While O_{PP} exceeding 4.3%, the SnO_x:Ta layer tends to have high resistance, possibly because of its poor crystallinity. Changing channel thicknesses *d* of the SnO_x and SnO_x:Ta TFTs, Fig. 1(d) and Table 1 illustrate the corresponding transfer characteristics and electrical parameters, e.g. μ_{FET}, SS, on/off current ratio ($I_{on/off}$). For the undoped SnO_x TFTs, the μ_{FET} increases from 0.69 to 1.11 $cm^2/(V\cdot s)$ while increasing *d* from 20 to 28 nm. The $I_{on/off}$ shows its strong dependence on *d* and gets reduced from 3.60×10^3 to 1.27×10^2. In contrast, with Ta incorporation, the SnO_x:Ta TFTs exhibit the improved $I_{on/off}$ at the level of 10^4, as well as the suppressed SS. Therefore, the p-type MO films are deposited at O_{PP} = 3.3% and with the thickness of 24 nm, and a thermal annealing is implemented for optimizing electrical performance of the fabricated TFTs, 250 °C for the undoped SnO_x and 270 °C for the doped SnO_x:Ta in our next discussions.

To further illustrate the effect of Ta doping on SnO_x thin films, the GIXRD patterns of the SnO_x and SnO_x:Ta films after annealing are presented in Fig. 2(a). Here, the (110) diffraction peaks of the *α*-SnO phase observed in the SnO_x and SnO_x:Ta films, indicates the crystalline formation[17]. The (0 0 12) diffraction peak of the Ta_2O_5 phase demonstrates the effective incorporation of Ta dopants in the SnO_x:Ta film. Meanwhile, increasing annealing duration from 10 to 30 min for SnO_x or after Ta doping, we observe that the (110) diffraction peaks become weaker, indicating the weakened formation of the *α*-SnO crystallization. The insets to Fig. 2(a) show atomic force microscopy (AFM) images of the MO films after the 30-min annealing, in which the extracted root-mean-square roughness is 4.4 nm for the SnO_x film, and 8.3 nm for the SnO_x:Ta film respectively. These can be attributed to the crystalline phase of Ta_2O_5 and a larger grain size of the SnO_x:Ta films, where the formation of Ta=O strong bonds improve film quality[18, 19]. Herein, the enhanced surface roughness could impact contact between the semiconductor channel and the metal electrode[20], and results in a large contact resistance in the SnO_x:Ta TFTs.

Furthermore, chemical compositions of the SnO_x films after the 10-min and 30-min annealing, the SnO_x:Ta after the 30-min annealing are analyzed by XPS in Fig. 2(b), where an *in-situ* etch (60 s, Ar^+ ion) is carried out before the spectrum acquisition[21]. After Gaussian fitting, the O 1*s* peak can be divided into three sub-peaks, located at 530.4, 531.8, and 533.0 eV[22]. The three fit sub-peaks are lattice oxygen (O_{Latt}), oxygen vacancy (O_{Vac}), and dissociated oxygen (O_{Chem}), respectively. The Sn 3*d* spectrum consists of the Sn^0 peak located at 484.4, the Sn^{2+} peak at 485.9, and the Sn^{4+} peak at 486.6 eV[17]. While increasing annealing duration (from 10 to 30 min) for the SnO_x films, the area percentage of O_{Vac} gets decreased from 78.14% to 12.58%. However, a high ratio of O_{Chem} (76.41%) in the SnO_x films after the 30-min annealing indicates that high-density defect states still exist in the annealed SnO_x films. The SnO_x:Ta film presents the highest ratio of O_{Latt}, with an area percentage of 38.07%, and the low oxygen vacancy (O_{Vac}, 20.07%), indicating the defect states concentration being decreased via Ta incorporation. Meanwhile, in the Sn 3*d* spectra, the Sn^{4+} peak is notably lower in the SnO_x:Ta films (Sn^{4+} = 25.12%) than in those undoped SnO_x films (Sn^{4+} = 31.66% for the 30-min annealing, 58.47% for the 10-min annealing), i.e. the Sn^{2+} states get oxidized less easily after Ta doping. The area percentages of all the combined peaks by deconvoluting the XPS O 1*s* and Sn 3*d* spectra profile are listed in Table 2.

Transmittance spectra of the SnO_x and SnO_x:Ta films are measured in Fig. 2(c), the inset displays the $(ahυ)^{1/2}$ versus *hυ* curves. Here, *α* is the energy-dependent absorption coefficient, *hυ* is the incident photon energy. Based on the Tauc method, *α* can be expressed by the following equation[23]:

$$ahv = C(hv - E)^{\gamma}, \quad (1)$$

where *h* is the Planck constant, *v* is the photon's frequency, *E* is the band gap energy, and *C* is a constant. The factor *γ* depends on the nature of electron transition and is equal to 1/2 or 2 for the direct and indirect band gaps, respectively. Here, based on Tauc plot of inset of Fig. 2(c) and Eq. (1), the indirect, optical band gaps are calculated to be 1.29 eV for the SnO_x films, and 1.98 eV for the SnO_x:Ta films. Consequently, the enlarged band gap can ensure a low off-state current (I_{off})[8], which is in good agreement with the observations of Fig. 1(d) for the SnO_x and SnO_x:Ta TFTs.

To quantitatively evaluate the interface quality of the p-type MO films, the conductance method is utilized in the

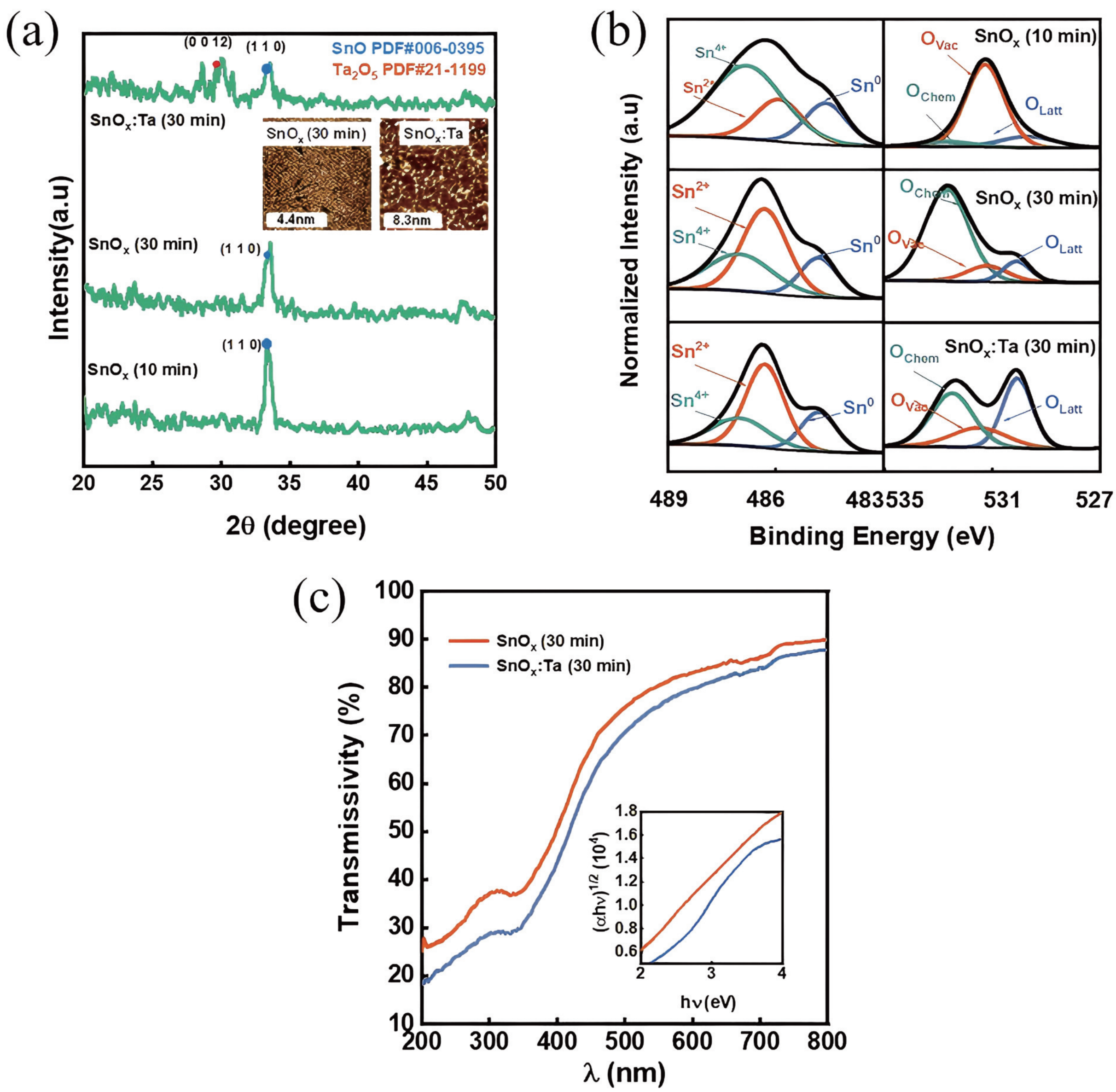

Fig. 2. (Color online) (a) GIXRD patterns of the SnO_x/SnO_x:Ta films, the insets display AFM images. (b) XPS spectra of the Sn 3*d* orbitals and O 1*s* core-level. (c) Transmittance spectra; the inset shows $(ah\upsilon)^{1/2}$ versus $h\upsilon$ plots.

SnO_x and SnO_x:Ta-based MOSCAPs. As the capacitor structure depicted in inset, Fig. 3(a) shows depletion capacitance (C_P) and conductance (G/ω) versus voltage curves, which are measured at a typical low frequency range of 600–800 Hz by using single scan mode from inversion to accumulation. Here, the interface state density (D_{it}) can be estimated from the normalized parallel conductance peak $(G_P/\omega)_{max}$[24, 25]:

$$D_{it} = \frac{2.5}{Aq}\left(\frac{G_P}{\omega}\right)_{max}, \quad (2)$$

where A is the device area, q is the electron charge, and $(G_P/\omega)_{max}$ is the maximum value of G_P/ω–V curve at single frequency f. We extract the D_{it} maxima of 3.25×10^{12} and 4.25×10^{12} $cm^{-2}\cdot eV^{-1}$ for SnO_x:Ta and SnO_x, respectively at $(G_P/\omega)_{max}$ = 753.93 and 982.38 pF. Here, G_P/ω is defined as: $G_P/\omega = \omega C_{OX}^2 G/(G^2 + \omega^2(C_{OX} - C_P)^2)$, C_{OX} is the oxide capacitance, ω is the angular frequency $\omega = 2\pi f$. This result is consistent with the decreased O_{Vac} and the enhanced O_{Latt} in SnO_x:Ta, where the Ta=O bonds increase stability of the lattice structure and effectively reduce the defects density[25].

Next, to investigate the impact of Ta incorporation on electrical performance of the SnO_x TFTs, representative transfer characteristics (I_{DS}–V_{GS}) of the undoped SnO_x and doped SnO_x:Ta TFTs with the W/L ratio ranging from 1 to 20 are illustrated in Fig. 3(b). Here, the channel length is fixed at 30 μm, and the devices are measured under atmospheric conditions and at V_{DS} = –1 V. Electrical parameters with respect to I_{off}, on/off current ratio ($I_{on/off}$), μ_{FET}, and SS are fully depicted in Figs. 3(c) and 3(d). In the p-type SnO_x TFTs, I_{off} increases as W/L increases from 1 to 20, and is reduced by annealing and Ta doping. Increasing the annealing duration, I_{off} of the SnO_x TFTs decreases, because of the reduced O_{Vac} that acts as donor-like defect and can contribute to electron carriers of channel and I_{off}[26]. Furthermore, the SnO_x:Ta TFTs with 30-min annealing presents the smallest value (~10^{-12} A/μm) of I_{off}, the highest on/off current ratio (~10^4) and the lower dependence on W/L, because the Ta=O strong bonds have led to the decreased O_{Chem} (Fig. 2(b)) that is relevant to the acceptor-like oxygen interstitials and provides intrinsic holes to the SnO_x films[27]. From another aspect, SS of the undoped

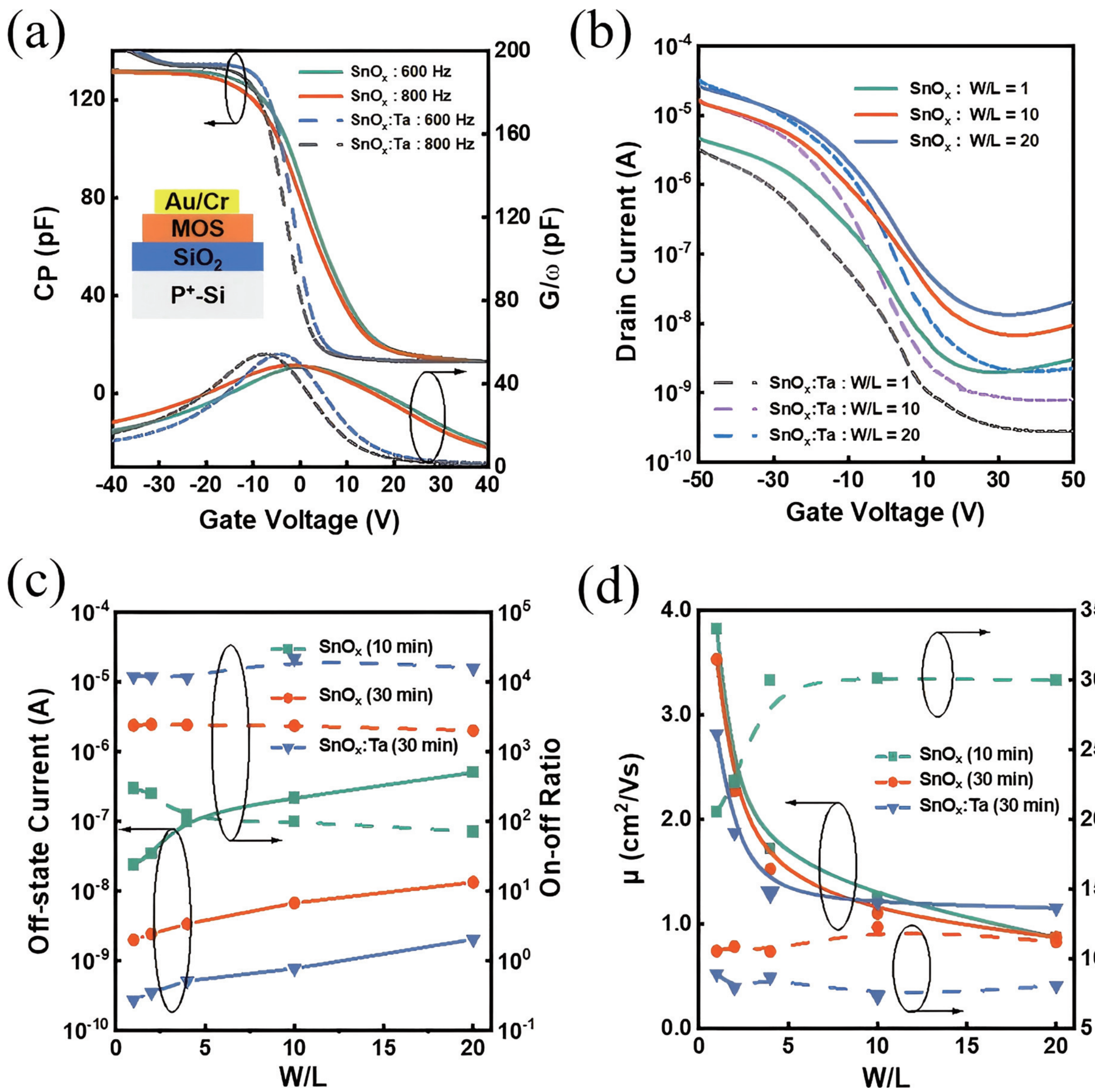

Fig. 3. (Color online) (a) Capacitance (C_P) and conductance (G/ω) as a function of gate voltage V_{GS}, in the SnO_x/SnO_x:Ta MOSCAPs after annealing for 30 min. (b) I_{DS}–V_{GS} curves (V_{DS} = −1 V) of the SnO_x and SnO_x:Ta TFTs. (c) Off-state current and on/off ratio. (d) μ_{FET} and SS.

SnO_x TFTs can be improved from ~30 to ~10 V/dec (Fig. 3(d)) with the increased annealing duration, suggesting the reduced defect states density. More importantly, the doped SnO_x:Ta TFTs exhibit the SS values of ~7 V/dec, demonstrating that Ta incorporation can effectively reduce D_{it}. These are well consistent with the D_{it} calculations based on the C–V and G–V measurements beforementioned.

As reported in many literatures[27–29], the unpattern semiconductor channel layers or gate dielectrics are often employed in the MO TFTs, where the fringe current effect is inevitably presented and affects the mobility evaluation thereafter. In Fig. 3(d), it can be seen that μ_{FET} in the SnO_x and SnO_x:Ta TFTs decreases close to the real value while W/L increasing from 1 to 2, 4, 10, and 20. However, the SnO_x:Ta TFTs presents the weakest fringe effect, attributed to its larger contact resistance and lower defect density[28, 30]. In p-type SnO_x:Ta TFTs with the relatively good uniformity, we conclude that a large W/L over 10 is essential to alleviate the fringe effect. Also, for the case of W/L = 10, electrical performances of the SnO_x:Ta TFTs have been observed with the enhanced on/off current ratio of 2.17 × 10^4, the optimized SS

Table 3. Key parameters for TCAD simulation.

Symbols (Unit)	SnO_x	SnO_x:Ta
N_{TA} ($cm^{-3}\cdot eV^{-1}$)	2.43 × 10^{20}	2.43 × 10^{20}
N_{TD} ($cm^{-3}\cdot eV^{-1}$)	2.50 × 10^{21}	2.50 × 10^{21}
N_{GD} ($cm^{-3}\cdot eV^{-1}$)	0.80 × 10^{18}	1.70 × 10^{18}
N_{GA} ($cm^{-3}\cdot eV^{-1}$)	0.95 × 10^{19}	0.98 × 10^{19}
E_{GD} (eV)	1.29	1.29
E_{GA} (eV)	0.77	0.77
R_c (Ω·μm)	1.2 × 10^4	0.8 × 10^4

value of 7.24 V/dec (decreased by 41%), and the suppressed fringe effect where μ_{FET} gets decreasing from 2.82 to 1.15 cm^2/(V·s), in comparison with the correspondingly parameters (2.34 × 10^3, 12.25 V/dec and 3.53 to 0.87 cm^2/(V·s)) of the undoped SnO_x TFTs after the 30-min annealing.

To deeply understand fringe effect in the SnO_x TFTs, detailed simulations are conducted in Fig. 4, by using Atlas/TCAD simulator[31]. The three-dimensional geometry of the SnO_x-based TFTs is congruent with the experimental configuration, with W/L = 1 and 20. And the channel length is fixed at

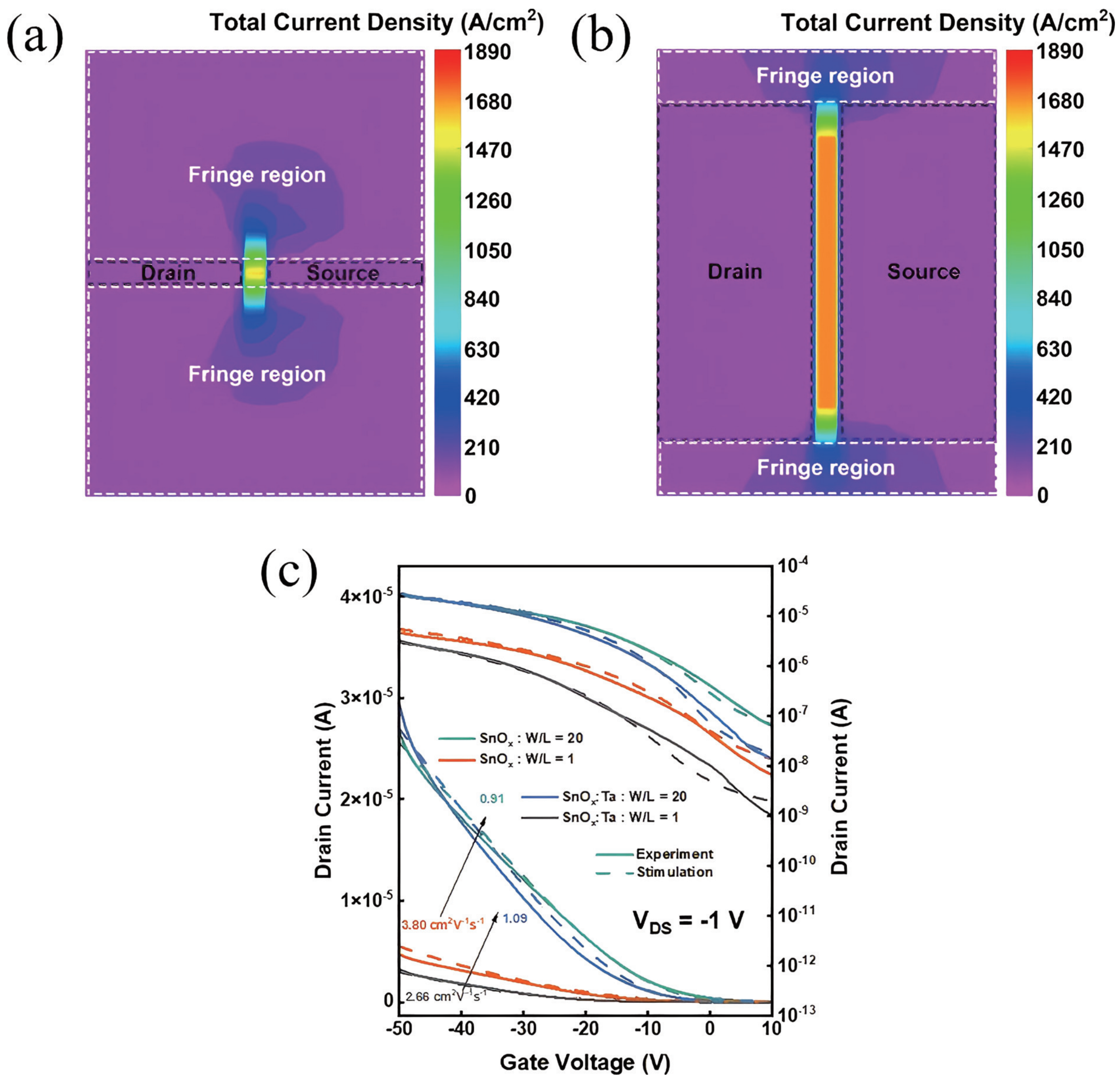

Fig. 4. (Color online) Current (in A/cm^2) distribution inside channel and fringe region of the SnO_x TFTs with (a) W/L = 1 and (b) W/L = 20 in the on-state (V_{GS} = −50 V, V_{DS} = −1 V). (c) Simulated and measured transfer characteristics (V_{DS} = −1 V) for the SnO_x TFTs with and without doping.

30 m. The density of states (DOS) utilized to model the experimental data include the acceptor-like Gaussian states, which are located at 0.52 eV above the valence band minimum (VBM), 9.0 × 10^{18} for SnO_x:Ta and 9.5 × 10^{18} $cm^{-3}{\cdot}eV^{-1}$ for SnO_x, along with donor-like Gaussian states (N_{GD}) at 1.29 eV above the VBM with densities of 1.7 × 10^{18} for SnO_x:Ta and 0.8 × 10^{18} $cm^{-3}{\cdot}eV^{-1}$ for SnO_x. Donor-like tail states (N_{TD}) and acceptor-like tail states (N_{TA}) in bulk, source/drain contact resistance (R_C) are also included in the model[32]. Moreover, the interfacial tail states (D_{it}), i.e. 3.25 × 10^{12} and 4.25 × 10^{12} $cm^{-2}{\cdot}eV^{-1}$ for SnO_x:Ta and SnO_x respectively, are also taken into account for SnO_x:Ta and SnO_x, based on our experimental extraction and the D_{it} maxima beforementioned. The key parameters for TCAD simulations are detailly illustrated in Table 3. The higher current inside the fringe region is presented in W/L = 1 (Fig. 4(a)), compared to that of W/L = 20 (Fig. 4(b)), validating the fringe effect inside the SnO_x TFTs. Furthermore, as W/L increases from 1 to 20, the mobility decreases from 2.66 to 1.09 $cm^2/(V{\cdot}s)$ in the SnO_x:Ta TFTs, and from 3.80 to 0.91 $cm^2/(V{\cdot}s)$ in the case of SnO_x. This observation proves that Ta incorporation effectively suppressed fringe effect within the film by promoting an increase in contact resistance and reduction of defect states density.

To study the device stability, all the p-type MO TFTs are measured under a negative gate bias of −20 V for varied stress duration (0–3600 s). The TFT transfer characteristics are obtained under operation temperatures of 300 and 330 K, as shown in Figs. 5(a) and 5(b). Threshold voltage shift (ΔVth) of the SnO_x:Ta TFTs has been improved from −2.47 to −1.76 V at 300 K (from −4.03 to −2.80 V at 330 K), in comparison to those of the undoped SnO_x TFTs. The lower ΔVth of SnO_x:Ta TFTs demonstrates the enhanced stability via Ta incorporation, and suggests that less defects are generated in the channel layer and interface regions during the bias stressing[33]. Correspondingly, Fig. 5(c) illustrates I_{off} as a function of stress duration. I_{off} of the SnO_x:Ta TFTs maintain relatively low values, regardless of the stress duration and temperature, proving the enlarged band gap to suppress the intrinsic excitation after Ta doping. Finally, environmental stability is shown in Fig. 5(d). After being exposed in ambient for 30 days, the

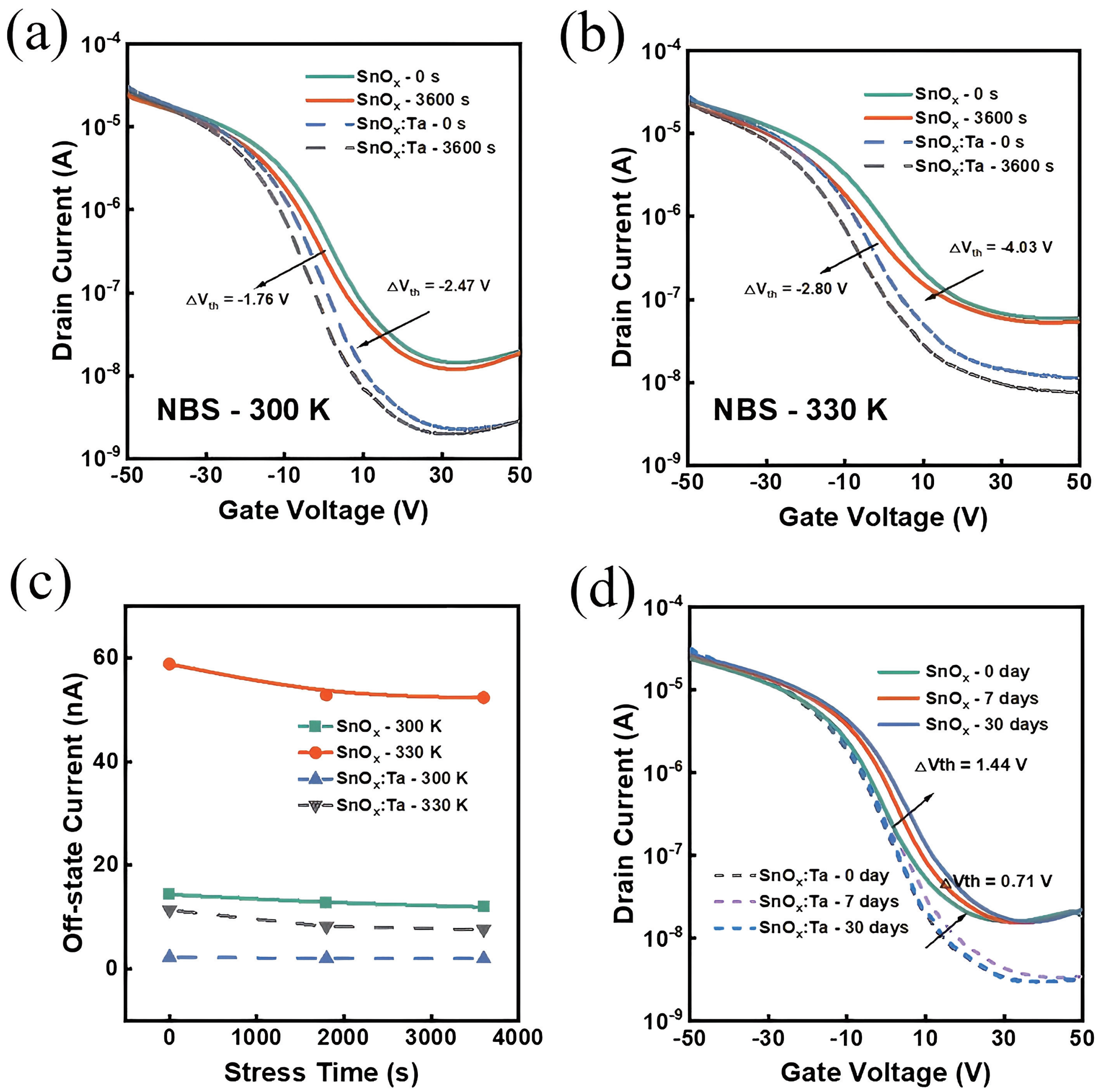

Fig. 5. Transfer characteristics of the SnO_x and SnO_x:Ta TFTs after annealing for 30 min under NBS (V_{GS} = −20 V, V_{DS} = −1 V) at 300 K (a) and 330 K (b). (c) Off-state current as a function of NBS stress duration, at 300 and 330 K. (d) I_{DS}–V_{GS} curves of the TFTs after 30 days of exposure in ambient air.

ΔVth is 1.44 V for the SnO_x TFTs and 0.71 V for the SnO_x:Ta TFTs. According the trend of ΔVth shift in the SnO_x:Ta TFTs, the superior stability can be maintained even after 100 days. Here, the improved environmental stability and ΔVth in the SnO_x:Ta TFTs is primarily attributed to the reduced surface defect states and roughness, which alleviate the absorption of oxygen and water that deplete the electron carriers[34, 35].

4. Conclusion

To sum up, we demonstrate Ta incorporation into the p-type SnO_x film and transistors for the first time, and investigate their semiconducting characteristics based on RF magnetron sputtering. Due to the introduction of Ta element, a higher annealing temperature (270 °C) is needed for optimizing the film quality and electrical performance of the SnO_x TFTs. Through XRD and AFM characterizations, we have observed the improved crystallinity and grain size in the SnO_x film upon Ta doping. And the reduction of defect density in the doped SnO_x:Ta films is demonstrated by XPS, C–V and G–V measurements. Band gap of the SnO_x film has been widened from 1.29 to 1.98 eV via Ta incorporation. Electrical performance of the SnO_x:Ta TFTs, including the I_{off} (down to 10^{-12} A/μm), on/off current ratio (2.17 × 10^4) and SS (decreased by 41%, comparing to that of the undoped SnO_x TFTs), was impressively improved. As well, fringe effect has been mitigated via Ta incorporation, facilitating accurate mobility calculations in the SnO_x-based TFTs. The SnO_x:Ta TFTs presents the obviously enhanced stability under NBS and NBTS, and exhibit long-term stability upon environmental exposure. This work provides an effective method to improve electrical characteristics of the p-type SnO_x TFTs by Ta doping, which can be helpful for their further exploration and development.

Acknowledgments

This work was supported in part by National Key R&D Program of China (Grant No. 2022YFE0141500), National Natural

Science Foundation of China (Grant Nos. 62004065 and 62274059).

References

[1] Wang Z W, Nayak P K, Caraveo-Frescas J A, et al. Recent developments in p-type oxide semiconductor materials and devices. Adv Mater, 2016, 28(20), 3831

[2] Jeong H, Kong C S, Chang S W, et al. Temperature sensor made of amorphous indium–gallium–zinc oxide TFTs. IEEE Electron Device Lett, 2013, 34(12), 1569

[3] Hung M H, Chen C H, Lai Y C, et al. Ultra low voltage 1-V RFID tag implement in a-IGZO TFT technology on plastic. 2017 IEEE International Conference on RFID (RFID), 2017, 193

[4] Zhang W, Liang R R, Liu L B, et al. Demonstration of α-InGaZnO TFT nonvolatile memory using TiAlO charge trapping layer. IEEE Trans Nanotechnol, 2018, 17(6), 1089

[5] Shiah Y S, Sim K, Shi Y H, et al. Mobility–stability trade-off in oxide thin-film transistors. Nat Electron, 2021, 4, 800

[6] Nomura K, Kamiya T, Hosono H. Ambipolar oxide thin-film transistor. Adv Mater, 2011, 23(30), 3431

[7] Caraveo-Frescas J A, Nayak P K, Al-Jawhari H A, et al. Record mobility in transparent p-type tin monoxide films and devices by phase engineering. ACS Nano, 2013, 7(6), 5160

[8] Hu Y Q, Yao X L, Schlom D G, et al. First principles design of high hole mobility p-type Sn–O–*X* ternary oxides: Valence orbital engineering of Sn^{2+} in Sn^{2+}–O–*X* by selection of appropriate elements *X*. Chem Mater, 2021, 33(1), 212

[9] Hsu S M, Yang C E, Lu M H, et al. Mobility enhancement in P-type SnO thin-film transistors *via* Ni incorporation by co-sputtering. IEEE Electron Device Lett, 2022, 43(2), 228

[10] Qin L, Yuan S G, Chen Z Q, et al. Solution-processed transparent p-type orthorhombic K doped SnO films and their application in a phototransistor. Nanoscale, 2022, 14(37), 13763

[11] Zhang Z F, Guo Y Z, Robertson J. P-type semiconduction in oxides with cation lone pairs. Chem Mater, 2022, 34(2), 643

[12] Hu Y Q, Hwang J, Lee Y, et al. First principles calculations of intrinsic mobilities in tin-based oxide semiconductors SnO, SnO_2, and Ta_2SnO_6. J Appl Phys, 2019, 126(18), 185701

[13] Hu Y Q, Schlom D, Datta S, et al. Amorphous Ta_2SnO_6: A hole-dopable p-type oxide. Appl Surf Sci, 2023, 613, 155981

[14] Barone M, Foody M, Hu Y Q, et al. Growth of Ta_2SnO_6 films, a candidate wide-band-gap p-type oxide. J Phys Chem C, 2022, 126(7), 3764

[15] Huang A P, Chu P K. Crystallization improvement of Ta_2O_5 thin films by the addition of water vapor. J Cryst Growth, 2005, 274(1/2), 73

[16] Huang A P, Xu S L, Zhu M K, et al. Crystallization control of sputtered Ta_2O_5 thin films by substrate bias. Appl Phys Lett, 2003, 83(16), 3278

[17] Zhou Y Y, Song Y, Hong R H, et al. Electrical evolution of p-type SnOx film and transistor deposited by RF magnetron sputtering. IEEE Trans Electron Devices, 2023, 70(6), 3100

[18] Perron A, Politano O, Vignal V. Grain size, stress and surface roughness. Surf Interface Anal, 2008, 40(3/4), 518

[19] Ono H, Koyanagi K I. Infrared absorption peak due to Ta=O bonds in Ta_2O_5 thin films. Appl Phys Lett, 2000, 77(10), 1431

[20] Zhao Y P, Wang Z X, Xu G W, et al. High performance indium-gallium-zinc oxide thin film transistor *via* interface engineering. Adv Funct Mater, 2020, 30(34), 2003285

[21] Lee S J, Jang Y, Kim H J, et al. Composition, microstructure, and electrical performance of sputtered SnO thin films for p-type oxide semiconductor. ACS Appl Mater Interfaces, 2018, 10(4), 3810

[22] Bae K H, Shin M G, Hwang S H, et al. Electrical performance and stability improvement of p-channel SnO thin-film transistors using atomic-layer-deposited Al_2O_3 capping layer. IEEE Access, 2020, 8, 222410

[23] Makuła P, Pacia M, Macyk W. How to correctly determine the band gap energy of modified semiconductor photocatalysts based on UV-vis spectra. J Phys Chem Lett, 2018, 9(23), 6814

[24] Qiao L S, He G, Hao L, et al. Interface optimization of passivated Er_2O_3/Al_2O_3/InP MOS capacitors and modulation of leakage current conduction mechanism. IEEE Trans Electron Devices, 2021, 68(6), 2899

[25] Yan Y Y, Kilchytska V, Flandre D, et al. Investigation and optimization of traps properties in Al_2O_3/SiO_2 dielectric stacks using conductance method. Solid State Electron, 2022, 194, 108347

[26] Han S, Flewitt A J. The origin of the high off-state current in p-type Cu_2O thin film transistors. IEEE Electron Device Lett, 2017, 38(10), 1394

[27] Chen C D, Chen Z H, Xu K J, et al. Thin-film transistors with the fringe effect and the correction factor for mobility extraction. IEEE Electron Device Lett, 2019, 40(6), 897

[28] Pei K, Chen M, Zhou Z W, et al. Overestimation of carrier mobility in organic thin film transistors due to unaccounted fringe currents. ACS Appl Electron Mater, 2019, 1(3), 379

[29] Okamura K, Nikolova D, Mechau N, et al. Appropriate choice of channel ratio in thin-film transistors for the exact determination of field-effect mobility. Appl Phys Lett, 2009, 94(18), 183503

[30] Huang C H, Tang Y L, Yang T Y, et al. Atomically thin tin monoxide-based p-channel thin-film transistor and a low-power complementary inverter. ACS Appl Mater Interfaces, 2021, 13(44), 52783

[31] Atlas user's manual: device simulation software (Silvaco Inc., Santa Clara, CA, 2019)

[32] Rajshekar K, Hsu H H, Kumar K U M, et al. Effect of plasma fluorination in p-type SnO TFTs: Experiments, modeling, and simulation. IEEE Trans Electron Devices, 2019, 66(3), 1314

[33] Shi Y P, Liu G X, Wu X M, et al. UV-ozone-assisted solution-processed high-k ZrO_2 for MoS_2 field-effect transistors. IEEE Trans Electron Devices, 2024, 71(4), 2789

[34] Qu Y X, Yang J, Li Y P, et al. Organic and inorganic passivation of p-type SnO thin-film transistors with different active layer thicknesses. Semicond Sci Technol, 2018, 33(7), 075001

[35] Park J S, Jeong J K, Chung H J, et al. Electronic transport properties of amorphous indium-gallium-zinc oxide semiconductor upon exposure to water. Appl Phys Lett, 2008, 92(7), 072104

Yu Song received his BS degrees Electronic Information Engineering from Hunan University of Information Technology. Now, he is a PhD student at the School of Physics and Electronics, Hunan University under the supervision of Professor Guoli Li. His research focuses on p-type metal oxide thin film transistors.

Guoli Li received the dual Ph.D. degrees in Electrical Engineering from Université catholique de Louvain (Belgium) and in Circuits and Systems from Hunan University in 2017. She currently serves as an associate Professor at the College of Semiconductors (College of Integrated Circuits), Hunan University. And her primary research focuses on thin-film transistors and device modeling.